CrystEngComm

ROYAL SOCIETY OF CHEMISTRY

COMMUNICATION

View Article Online
View Journal | View Issue



Cite this: *CrystEngComm*, 2024, **26**, 6269

Received 7th October 2024,
Accepted 25th October 2024

DOI: 10.1039/d4ce01023j

rsc.li/crystengcomm

# Structural transformation of silver(I)–thiolate coordination polymer film at solid–liquid interfaces†

Myu Fukuoka,[a] Yohei Takashima,[a] Kensuke Akamatsu,[a] Aude Demessence[b] and Takaaki Tsuruoka*[a]

**We report that the ligand-exchange reaction between [Ag(*o*-SPhCO$_2$H)]$_n$ deposited on a solid substrate and the free *p*-HSPhCOOH ligand in solution results in crystal transformation from [Ag(*o*-SPhCO$_2$H)]$_n$ to [Ag(*p*-SPhCO$_2$H)]$_n$ on the substrate. Structural analysis revealed a structural transformation between CPs with different topologies *via* ligand exchange.**

As a nascent category of crystalline inorganic–organic hybrid materials, coordination polymers (CPs) have garnered considerable interest owing to their distinctive topologies and prospective applications in diverse fields, including gas storage and separation,[1–6] sensing,[7–9] catalysis,[10–12] and drug delivery.[13–15] The structural configuration of the resulting CPs appears to be a critical determinant of their electronic, optical, and magnetic properties.[16–22] Even minor alterations to their structural configuration can significantly impact the properties of the resulting CPs.

Several studies have investigated the structural transformation of CPs through alterations in the counter anion, solvent, metal ion, and ligand.[23–28] Although the structural transformation of CPs is based on the rearrangement of metal clusters and ligands through the cleavage of coordination bonds or structural change of metal clusters, predicting such structural transformations remains challenging. Hence, several researchers have focused on identifying the factors that induce structural transformation.[29–32] To date, solvent-assisted ligand exchange (SALE) represents one of the most effective strategies for controlling the structures and properties of CPs.[33] Although analogous ligands could be partially or completely introduced into the CP structure through competition between different ligands in solution, most reported SALEs involve transformations of porous CPs because the penetration of solvent and ligands into the CPs is key for structural transformation. In contrast, in the case of ligand exchange for non-porous CPs by immersion of CP crystals into the ligand solution, the reaction proceeds in a heterogeneous system at the interface between the surface of the CP crystals and the solution comprising ligands.[29–32] While the ligand exchange mechanism of porous CPs in a quasi-homogeneous reaction system has been extensively studied, the ligand exchange processes of non-porous CPs remain unclear owing to the lack of an appropriate protocol. Therefore, developing a comprehensive and straightforward approach to regulating ligand-exchange processes could provide the foundation for an improved understanding of the ligand-exchange mechanisms of CPs.

Herein, we propose a promising and straightforward strategy for the structural transformation of Ag thiolate CPs *via* ligand exchange on substrates. This strategy involves the preparation of [Ag(*o*-SPhCO$_2$H)]$_n$ (*o*-SPhCOOH: *ortho*-mercaptobenzonate) using an Ag$^+$-doped organic polymer substrate, followed by a ligand-exchange reaction at

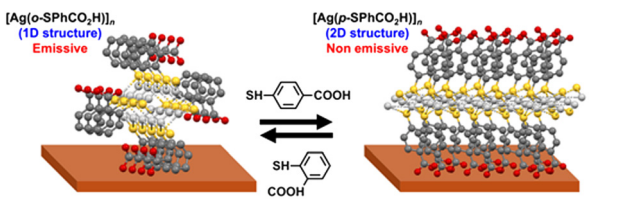


**Scheme 1** Schematic illustration of the structure and the ligand-exchange reaction between [Ag(*o*-SPhCO$_2$H)]$_n$ and [Ag(*p*-SPhCO$_2$H)]$_n$ CPs. White, Ag; yellow, S; red, O; gray, C.

[a] *Department of Nanobiochemistry, Frontiers of Innovative Research in Science and Technology (FIRST), Konan University, 7-1-20 Minatojimaminami, Chuo-ku, Kobe 650-0047, Japan. E-mail: tsuruoka@konan-u.ac.jp*
[b] *Université Claude Bernard Lyon 1, CNRS, Institut de Recherches sur la Catalyse et l'Environnement de Lyon (IRCELYON), UMR 5256, Villeurbanne, France*

† Electronic supplementary information (ESI) available: Experimental; schematic illustration of the formation of [Ag(*o*-SPhCO$_2$H)]$_n$ CPs; SEM image, XRD pattern, and emission spectrum of [Ag(*o*-SPhCO$_2$H)]$_n$ CPs obtained by microwave irradiation using the Ag$^+$-doped polyimide film; influence of ligand concentrations on ligand-exchange rate and surface morphology of the obtained samples; schematic illustration of the crystal conversion by the ligand exchange. See DOI: https://doi.org/10.1039/d4ce01023j

the interface between $[Ag(o\text{-}SPhCO_2H)]_n$ on the substrate and *p*-HSPhCOOH (*p*-HSPhCOOH: *para*-mercaptobenzoic acid) in solution. The transformation from 1D $[Ag(o\text{-}SPhCO_2H)]_n$ to 2D $[Ag(p\text{-}SPhCO_2H)]_n$ in the present approach occurred on the surface of the initially formed $[Ag(o\text{-}SPhCO_2H)]_n$ crystals (Scheme 1). Furthermore, time-course analysis of the crystal structure, surface morphology, luminescent properties, and ligand composition of the resulting CP-based thin films suggested that structural transformation by the ligand exchange process occurred without the formation of an intermediate phase at the solid–liquid interfaces. This study elucidates the fundamental aspects of structural transformation by ligand exchange of non-porous CP crystals on the substrate and provides a potential pathway for preparing continuous free-standing CP crystal films by ligand exchange.

To form $[Ag(o\text{-}SPhCO_2H)]_n$ CP on the substrate, $Ag^+$-doped polyimide films were immersed in an aqueous solution containing the ligand, followed by heating at 180 °C for 60 min under microwave irradiation (Scheme S1†). The SEM images of the obtained samples (Fig. S1A†) reveal rod-shaped crystals with micrometer lengths formed on the substrate. In addition, the crystals were densely packed on the surfaces of the polyimide films. The powder XRD measurement showed that the peak positions of the obtained samples were consistent with those of the simulated pattern of the $[Ag(o\text{-}SPhCO_2H)]_n$ crystals, indicating that they exhibited the desired 1D crystal structure (Fig. S1B†).[34] Considering 1D $[Ag(o\text{-}SPhCO_2H)]_n$ crystals exhibit photoemission properties, the emission characterization of the obtained samples was also conducted in this experiment, which revealed that the crystals obtained on the substrate exhibited an emission peak at approximately 620 nm upon excitation at 365 nm (Fig. S1C†).

Ligand exchange of the Ag CPs was attempted by immersing the resulting $[Ag(o\text{-}SPhCO_2H)]_n$ crystal films in a methanol solution containing *p*-HSPhCOOH. In this reaction, the yellow $[Ag(o\text{-}SPhCO_2H)]_n$ crystals deposited on the film changed to white (Fig. 1A), indicative of $[Ag(p\text{-}SPhCO_2H)]_n$ crystals, thus indicating the success of the ligand-exchange reaction.[35] PXRD measurements showed that the pattern of the obtained sample after ligand exchange was consistent with the simulated pattern of the 2D $[Ag(p\text{-}SPhCO_2H)]_n$ crystals (Fig. 1B). The SEM images revealed that the rod-like crystals were composed of nanosized plate-like crystals (Fig. 1C). In addition, the sample before ligand exchange showed red emission under UV light irradiation at 365 nm, whereas the sample after ligand exchange showed no emission, consistent with the non-emissive behaviour of $[Ag(p\text{-}SPhCO_2H)]_n$ (Fig. 1D). Interestingly, the ligand-exchange reaction was carried out using a crystal film with partially exfoliated CP crystals, which retained their initial state after the reaction, suggesting that the ligand-exchange reaction proceeded directly on the surface of the CP crystals deposited on the substrate. These results demonstrated that the simple process of immersing the CP films in the ligand solution at 25 °C allowed the ligand-exchange reaction, resulting in the transformation of 1D $[Ag(o\text{-}SPhCO_2H)]_n$ to 2D $[Ag(p\text{-}SPhCO_2H)]_n$ crystals.

The concentration of the *p*-HSPhCOOH molecule was varied in the 5–20 mM range to evaluate the influence of the concentration of organic ligands on the exchange rate. When the ligand-exchange reaction progressed at a lower ligand concentration of 5 mM (standard condition: 10 mM), diffraction peaks derived from $[Ag(p\text{-}SPhCO_2H)]_n$ crystals were observed in the obtained sample after a reaction time of 120 min, whereas the peaks derived from the initial $[Ag(o\text{-}SPhCO_2H)]_n$ crystals remained (Fig. S2A†). In contrast, at the higher concentration of 20 mM, the peaks of the initial $[Ag(o\text{-}SPhCO_2H)]_n$ crystals completely disappeared in the sample with a reaction time of 80 min, with only the peaks derived from $[Ag(p\text{-}SPhCO_2H)]_n$ crystals observed (Fig. S2C†). These results indicate that the reaction rate depends on the ligand concentration. The SEM image of the sample obtained at a concentration of 5 mM showed plate-like crystals in the nanometer range sparsely formed on the initial $[Ag(o\text{-}SPhCO_2H)]_n$ crystals, indicating that the initial crystals remained partially intact. In contrast, SEM observations of the sample obtained at the higher ligand concentration of 20 mM showed that the rod morphology was maintained; however, the surface of the crystals was fully covered with plate-like crystals, indicating a completed ligand-exchange reaction (Fig. S2F†). Thus, the memory shape of the initial crystals was maintained.

To study the mechanism of ligand exchange using the present approach, we performed a time-course analysis of the ligand-exchange reaction using PXRD and emission measurements. The crystal structures of the samples during the ligand-exchange reaction are shown in Fig. 2A. The characteristic XRD peaks with the $2\theta$ degrees of 6.8° and 9.6° for the sample before the reaction can be assigned to the simulated pattern of the $[Ag(o\text{-}SPhCO_2H)]_n$ crystal. The intensities of these diffraction peaks decreased dramatically after 10 min and gradually decreased with increasing reaction time. In addition, after 120 min of reaction, the peaks disappeared completely. In contrast, after 10 min of reaction,

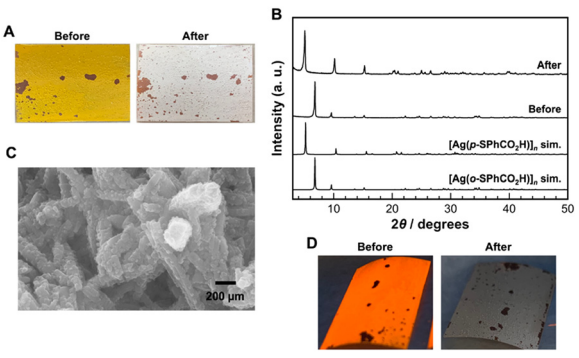


**Fig. 1** (A) Optical images, (B) XRD patterns, (C) SEM image, and (D) emission images under irradiation at 365 nm of the obtained samples before and after ligand exchange.

 

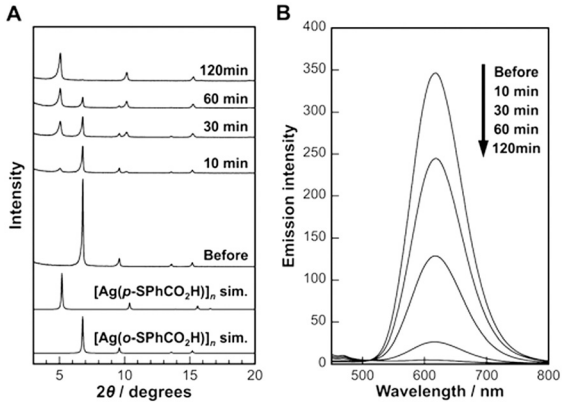


Fig. 2 (A) XRD patterns and (B) emission spectra of the obtained samples prepared under different reaction times (0–120 min).

two diffraction peaks with the $2\theta$ degrees of 5.2° and 10.4° were newly observed, corresponding to the $[Ag(p\text{-}SPhCO_2H)]_n$ crystal. The intensities of these diffraction peaks increased with the reaction time. In addition, only diffraction peaks originating from the $[Ag(o\text{-}SPhCO_2H)]_n$ and $[Ag(p\text{-}SPhCO_2H)]_n$ crystals were observed during this reaction, indicating that the $[Ag(o\text{-}SPhCO_2H)]_n$ crystals were directly converted to $[Ag(p\text{-}SPhCO_2H)]_n$ crystals without the formation of an intermediate state. Characterization of the emission properties of the sample confirmed that the intensity of the emission attributed to the $[Ag(o\text{-}SPhCO_2H)]_n$ crystals decreased with increasing reaction time, and the emission peak disappeared after 120 min (Fig. 2B), consistent with the PXRD measurement results.

Time-dependent changes in the surface morphology of the obtained samples during the ligand-exchange reaction are shown in Fig. 3. As mentioned above, the initial $[Ag(o\text{-}SPhCO_2H)]_n$ crystals exhibited a rod-like morphology with a smooth surface. Although the crystals retained their rod morphology after a reaction time of 10 min, new small crystals were formed on the surface of the initial crystals. After a reaction time of 60 min, the number and size of the crystals deposited on the surfaces of the initial crystals increased. For the sample with a reaction time of 120 min, although tetrahedral crystals were observed, the rod morphology, size, and number of crystals remained unchanged. The SEM observations and XRD measurements clearly indicate that $[Ag(p\text{-}SPhCO_2H)]_n$ crystals formed from the initial $[Ag(o\text{-}SPhCO_2H)]_n$ crystals *via* a ligand-exchange reaction. In addition, no crystals, except for $[Ag(p\text{-}SPhCO_2H)]_n$ crystals and eluted silver ions, were observed in the solution during the reaction, indicating that the initial 1D $[Ag(o\text{-}SPhCO_2H)]_n$ crystals directly converted to 2D $[Ag(p\text{-}SPhCO_2H)]_n$ crystals.

To gain further insight into the ligand-exchange process, we characterized the ratio of *p*-SPhCOOH to all ligands (*o*-SPhCOOH and *p*-SPhCOOH) in the crystals using NMR measurements. As shown in Fig. 4A, the ratio of *p*-SPhCOOH for all ligands increased dramatically in the early stages of the reaction, reaching approximately 0.68 at a reaction time of 30 min. After 30 min, the ratio gradually increased with reaction time. The rate of change in the ratio depended on the ligand concentration. At a lower ligand concentration of 5 mM, the ratio increased slowly up to 80 min and tended to saturate at 0.8, even at 120 min. At a higher concentration of 20 mM, the ratio increased rapidly at 30 min and reached almost 1 at 80 min. To confirm these changes in the ligand ratio, the changes in the emission intensity during the ligand-exchange reaction were also examined (Fig. 4B). The results showed that the emission intensity decreased dramatically in the initial reaction stage and then gradually decreased. In addition, the rate of decrease in the emission intensity increased with increasing ligand concentration. Based on these results, we propose a mechanism for the conversion of 1D $[Ag(o\text{-}SPhCO_2H)]_n$ crystals into 2D $[Ag(p\text{-}SPhCO_2H)]_n$ crystals *via* a ligand-exchange reaction (Scheme S2†). The ligand-exchange process proceeded preferentially on the surface of the initial $[Ag(o\text{-}SPhCO_2H)]_n$ crystals that formed on the substrate during the early stages of the reaction. The newly formed $[Ag(p\text{-}SPhCO_2H)]_n$ crystals covered the surfaces of the initial $[Ag(o\text{-}SPhCO_2H)]_n$ crystals. Finally, the initial $[Ag(o\text{-}SPhCO_2H)]_n$ crystals were completely converted

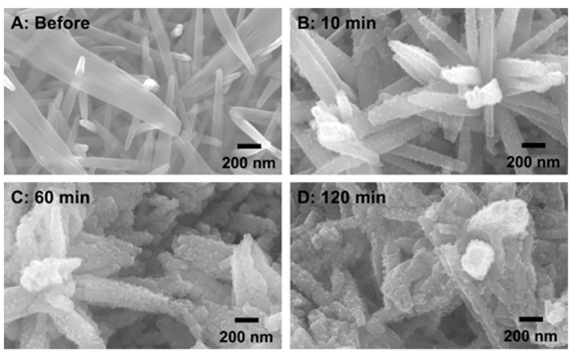


Fig. 3 SEM images of the obtained samples prepared under different reaction times (0–120 min).

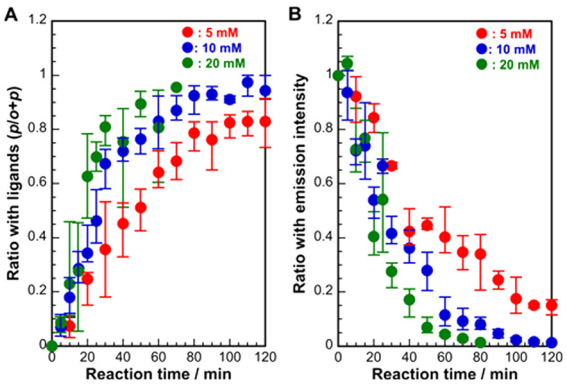


Fig. 4 Change in (A) ratio with ligands and (B) emission intensity of the crystals by using ligand exchange solution containing different concentrations of organic ligand as a function of reaction time.

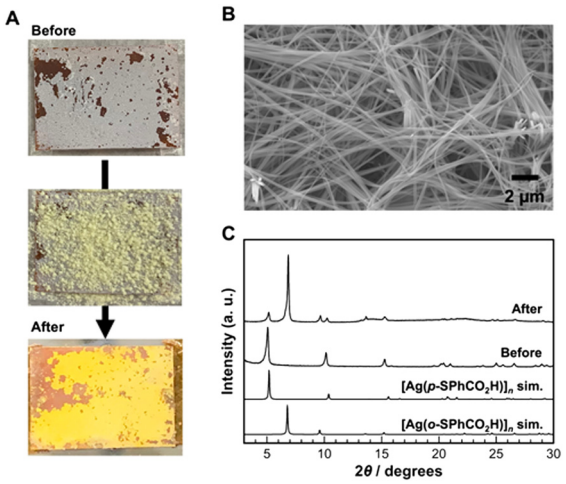


Fig. 5 (A) Optical images, (B) SEM image, and (C) XRD patterns of the obtained samples by the reverse ligand-exchange reaction.

to $[Ag(p\text{-}SPhCO_2H)]_n$ crystals as ligand exchange proceeded through the intercrystalline vacancies.

Subsequently, the immersion approach was applied to reverse ligand exchange from 2D $[Ag(p\text{-}SPhCO_2H)]_n$ to 1D $[Ag(o\text{-}SPhCO_2H)]_n$ CPs. However, the reverse ligand-exchange reaction did not proceed when the $[Ag(p\text{-}SPhCO_2H)]_n$ crystal film was immersed in a solution containing the *o*-HSPhCOOH ligand. This may be caused by the differences in the Ag–S bond distance. The Ag–S bond distances (Ag–S: 2.456, 2.493, 2.623 Å) in $[Ag(p\text{-}SPhCO_2H)]_n$ CP are slightly shorter than those of $[Ag(o\text{-}SPhCO_2H)]_n$ CP (Ag–S: 2.487, 2.560, 2.639 Å). In addition, the Ag–Ag bonds are formed in $[Ag(p\text{-}SPhCO_2H)]_n$ CP (Ag–Ag: 2.936 Å). These differences imply that $[Ag(p\text{-}SPhCO_2H)]_n$ CP may be thermodynamically more stable than $[Ag(o\text{-}SPhCO_2H)]_n$ CP. Therefore, instead of immersing the substrate in the solution, the ligand-exchange reaction was conducted in neat conditions by covering the $[Ag(p\text{-}SPhCO_2H)]_n$ crystal film with *o*-HSPhCOOH ligand powder and heating it at 180 °C for 12 h (melting point of *o*-HSPhCOOH ligand: 168 °C). Consequently, the colour of the crystals on the substrate changed from white to yellow, indicating the formation of $[Ag(o\text{-}SPhCO_2H)]_n$ CPs (Fig. 5A). SEM images of the obtained samples show that fiber-like crystals were formed on the substrate (Fig. 5B). The PXRD analysis of the sample obtained on the substrate clearly showed the formation of $[Ag(o\text{-}SPhCO_2H)]_n$ CPs (Fig. 5C). Moreover, the sharp diffraction peaks of the obtained samples indicated that the obtained CPs consisted of $[Ag(o\text{-}SPhCO_2H)]_n$ CPs with high crystallinity. However, the diffraction peaks of the $[Ag(p\text{-}SPhCO_2H)]_n$ CPs were observed in the sample after ligand exchange, indicating that not all $[Ag(p\text{-}SPhCO_2H)]_n$ crystals converted into $[Ag(o\text{-}SPhCO_2H)]_n$ crystals. This result implies that reversible crystal conversion based on ligand exchange between $[Ag(p\text{-}SPhCO_2H)]_n$ and $[Ag(o\text{-}SPhCO_2H)]_n$ CPs on the substrate is achievable using the present approach.

Herein, we proposed a unique ligand-exchange reaction between 2D $[Ag(p\text{-}SPhCO_2H)]_n$ and 1D $[Ag(o\text{-}SPhCO_2H)]_n$ CPs on a substrate and characterized their structural conversion. The crystal conversion from $[Ag(o\text{-}SPhCO_2H)]_n$ to $[Ag(p\text{-}SPhCO_2H)]_n$ CPs can be readily proceeded by immersing the $[Ag(o\text{-}SPhCO_2H)]_n$ CP film into the methanol solution containing *p*-HSPhCOOH ligands at 25 °C. In contrast, the reverse crystal conversion from $[Ag(p\text{-}SPhCO_2H)]_n$ to $[Ag(o\text{-}SPhCO_2H)]_n$ CPs requires the heating process at 180 °C. This difference in crystal conversion between the $[Ag(o\text{-}SPhCO_2H)]_n$ and $[Ag(p\text{-}SPhCO_2H)]_n$ CPs may be caused by the thermodynamic stability of these CPs. These results provide interesting insights into the structural transformation of CPs on substrates *via* ligand-exchange reactions.

This work was supported by JSPS KAKENHI Grant Number 23K04897 and Konan Advanced Research Project (Phase 1). We would like to thank Editage (**https://www.editage.jp**) for English language editing.

## Data availability

The data supporting this article have been included as part of the ESI.†

## Author contributions

M. F. performed the synthesis experiments and the characterization of the obtained samples. T. T. conceived the experiments and supervised the project. Y. T., K. A., D. A., and T. T. analyzed all date and discussed the mechanism for the crystal transformation. All authors contributed to the preparation of the manuscript.

## Conflicts of interest

There are no conflicts to declare.

## Notes and references

1 P. Kumar, K.-H. Kim, E. E. Kwon and J. E. Szulejko, *J. Mater. Chem. A*, 2015, **4**, 345–361.
2 B. Li, H.-M. Wen, Y. Yu, Y. Cui, W. Zhou, B. Chen and G. Qian, *Mater. Today Nano*, 2018, **2**, 21–49.
3 C. Gu, N. Hosono, J.-J. Zheng, Y. Sato, S. Kusaka, S. Sakai and S. Kitagawa, *Science*, 2019, **363**, 387–391.
4 Y.-Y. Xue, S.-N. Li, Y.-C. Jiang, M.-C. Hu and Q.-G. Zhai, *J. Mater. Chem. A*, 2019, **7**, 4640–4650.
5 J. Liu, Z. Lu, Z. Chen, M. Rimoldi, A. J. Howarth, H. Chen, S. Alayoglu, R. Q. Snurr, O. K. Farha and J. T. Hupp, *ACS Appl. Mater. Interfaces*, 2021, **13**, 20081–20093.
6 T. Jia, Y. Gu and F. Li, *J. Environ. Chem. Eng.*, 2022, **10**, 108300.
7 W. P. Lustig, S. Mukherjee, N. D. Rudd, A. V. Desai, J. Li and S. K. Ghosh, *Chem. Soc. Rev.*, 2017, **46**, 3242–3285.
8 S. Liu, J. Bai, Y. Huo, B. Ning, Y. Peng, S. Li, D. Han, W. Kang and Z. Gao, *Biosens. Bioelectron.*, 2020, **149**, 111801.

 

9 C.-Z. Wang, J. Chen, Q.-H. Li, G.-E. Wang, X.-L. Ye, J. Lv and G. Xu, *Angew. Chem., Int. Ed.*, 2023, **62**, e202302996.
10 J. Huang, Y. Li, R.-K. Huang, C.-T. He, L. Gong, Q. Hu, L. Wang, Y.-T. Xu, X.-Y. Tian, S.-Y. Liu, Z.-M. Ye, F. Wang, D.-D. Zhou, W.-X. Zhang and J.-P. Zhang, *Angew. Chem., Int. Ed.*, 2018, **57**, 4632–4636.
11 A. Singh, A. K. Singh, J. Lin and A. Kumar, *Catal. Sci. Technol.*, 2021, **11**, 3946–4989.
12 Z. Gao, L. Liang, X. Zhang, P. Xu and J. Sun, *ACS Appl. Mater. Interfaces*, 2021, **13**, 61334–61345.
13 L. Zhang, Z. Wang, Y. Zhang, F. Cao, K. Dong, J. Ren and X. Qu, *ACS Nano*, 2018, **12**, 10201–10211.
14 H. Wang, Y. Chen, H. Wang, X. Liu, X. Zhou and F. Wang, *Angew. Chem., Int. Ed.*, 2019, **58**, 7380–7384.
15 H. D. Lawson, S. P. Walton and C. Chan, *ACS Appl. Mater. Interfaces*, 2021, **13**, 7004–7020.
16 C. Lochenie, K. Schötz, F. Panzer, H. Kurz, B. Maier, F. Puchtler, S. Agarwal, A. Köhler and B. Weber, *J. Am. Chem. Soc.*, 2018, **140**, 700–709.
17 Y.-Q. Zhang, V. A. Blatov, T.-R. Zheng, C.-H. Yang, L.-L. Qian, K. Li, B.-L. Li and B. Wu, *Dalton Trans.*, 2018, **47**, 6189–6198.
18 J.-Y. Ge, Z. Chen, L. Zhang, X. Liang, J. Su, M. Kurmoo and J.-L. Zuo, *Angew. Chem., Int. Ed.*, 2019, **58**, 8789–8793.
19 L.-P. Tang, S. Yang, L. Dan, C. Wang, Y. Ge, L.-M. Tang, R.-L. Zhou and H. Zhang, *J. Mater. Chem. A*, 2020, **8**, 14356–14383.
20 R. G. Mariano, O. J. Wahab, J. A. Rabinowitz, J. Oppenheim, T. Chen, P. R. Unwin and M. Dincă, *ACS Cent. Sci.*, 2022, **8**, 975–982.
21 G. Valente, M. Esteve-Rochina, A. Paracana, A. Rodríguez-Diéguez, D. Choquesillo-Lazarte, E. Ortí, J. Calbo, M. Ilkaeva, L. Marfra, M. Hernández-Rodríguez, J. Rocha, H. Alves and M. Souto, *Mol. Syst. Des. Eng.*, 2022, **7**, 1065–1072.
22 C.-W. Lai, Y.-C. Lee, Y.-Z. Jiang, C.-H. Ling, G. Kumar, M. H. Huang and C.-T. Li, *J. Mater. Chem. A*, 2024, **12**, 1595–1608.
23 C. Tan, X. Han, Z. Li and Y. Cui, *J. Am. Chem. Soc.*, 2018, **140**, 16229–16236.
24 M. Taddei, R. J. Wakeham, A. Koutsianos, E. Andreoli and A. R. Barron, *Angew. Chem., Int. Ed.*, 2018, **57**, 11706–11710.
25 S. Zhao, C. Tan, C.-T. He, P. An, F. Xie, S. Jiang, Y. Zhu, K.-H. Wu, B. Zhang, H. Li, J. Zhang, Y. Chen, S. Liu, J. Dong and Z. Tang, *Nat. Energy*, 2020, **5**, 881–890.
26 T. He, X.-J. Kong, J. Zhou, K. Wang, X.-Q. Wu, X.-L. Lv, G.-R. Si, J.-R. Li and Z.-R. Nie, *J. Am. Chem. Soc.*, 2021, **143**, 9901–9911.
27 L. Zhang, J. Wang, H. Wang, W. Zhang, W. Zhu, T. Du, Y. Ni, X. Xie, J. Sun and J. Wang, *Nano Res.*, 2021, **14**, 1523–1532.
28 Y. Song, X. Liu, Z. Gao, Z. Wang, Y. Hu, K. Yang, Z. Zhao, D. Lan and G. Wu, *J. Colloid Interface Sci.*, 2022, **620**, 263–272.
29 G. Kang, Y. Jeon, K. Y. Lee, J. Kim and T. H. Kim, *Cryst. Growth Des.*, 2015, **15**, 5183–5187.
30 C.-T. Yang, X.-K. Yang, J.-H. Hu, W.-T. Lee, T.-R. Chen, C.-C. Wang and J.-D. Chen, *CrystEngComm*, 2020, **22**, 3322–3328.
31 L. Okhrimenko, C. C. Ndaya, A. Fateeva, G. Ledoux and A. Demessence, *New J. Chem.*, 2020, **44**, 17970–17975.
32 S. Hawila, F. Massuyeau, R. Gautier, A. Fateeva, S. Lebegue, W. Kim, G. Ledoux, A. Mesbah and A. Demessence, *J. Mater. Chem. B*, 2023, **11**, 3979–3984.
33 T. Islamoglu, S. Goswami, Z. Li, A. J. Howarth, O. K. Farha and J. T. Hupp, *Acc. Chem. Res.*, 2017, **50**, 805–813.
34 O. Veselska, N. Guillou, M. Diaz-Lopez, P. Bordet, G. Ledoux, S. Lebègue, A. Mesbah, A. Fateeva and A. Demessence, *ChemPhotoChem*, 2022, **6**, e202200030.
35 O. Veselska, C. Dessal, S. Melizi, N. Guillou, D. Podbevšek, G. Ledoux, E. Elkaim, A. Fateeva and A. Demessence, *Inorg. Chem.*, 2019, **58**, 99–105.